Lasers in Manufacturing Conference 2025

Investigating the Effect of Different Axial Oscillation Patterns on Laser Fusion Cutting Process

Busatto M.[1 *], Meyer J.[2], Caprio L.[1], Gandolfi D. [3], Herwig P.[2], Vanin M.[3], Previtali B.[1]

[1]*Department of Mechanical Engineering, Politecnico di Milano, Via La Masa 1, 20156 Milan, Italy*
[2]*Fraunhofer Institute for Material and Beam Technology IWS, Winterbergstr. 28, 01277 Dresden, Germany*
[3]*Adige S.P.A., BLM GROUP, Via per Barco 11, 38056 Levico Terme (TN), Italy*

Abstract

Latest research on laser cutting has revealed significant improvements in process productivity and cut quality through the applications of dynamic beam shaping techniques. The present work aims to study the effect of axial beam oscillations (along Z-axis) on laser fusion cutting process through analytical modelling and experimental investigations. While existing literature has primarily focused on dynamic beam shaping employing harmonic oscillations, this study explores the impact of various oscillation waveforms, including sinusoidal, triangular, square, ramp-up, and ramp-down patterns. Initially, an analytical model was developed to evaluate the laser intensity distribution within the process zone for different oscillation patterns. Furthermore, the effect of axial oscillations, superimposed on the cutting direction, was experimentally investigated using 20 mm thick AISI304 stainless steel. Experimental results demonstrate notable improvements in process performance through axial oscillation, either by reducing burr defects at the same processing speed or by increasing productivity while maintaining equivalent part quality.

Keywords: Laser cutting, Laser beam shaping, Laser beam axial oscillations, Waveforms;

1. Introduction

Today, laser cutting of metal materials stands out as one of the key applications in the manufacturing field.

Since its worldwide adoption in the metal-working industry, research has consistently aimed on enhance laser cutting process performances. In particular, recent advancements in laser cutting techniques utilizing novel dynamic beam shaping (DBS) methods have demonstrated substantial improvements in processing speed and cut quality of the manufactured parts (*Wetzig et al., 2020*). These techniques rely on the high-speed motion of laser beam, superimposed to the cutting direction. Laser oscillations around the kerf enable to shape the interaction zone into an arbitrary geometry while preserving the beam intensity distribution (*D'Arcangelo et al., 2024*).

Although significant improvements of process performances have been demonstrated using laser beam oscillations in the XY plane (*Goppold et al., 2019; Kardan et al., 2023*), to date, the application of fast focusing solutions for beam oscillation along the laser propagation direction (Z-axis) has been scarcely explored in literature.

Gropp et al. and *Okada et al.* were the first to show that the quick adaptation of the laser beam focal position is expected to enable an increase in processing speed and improvement in the quality of laser material processing (*Gropp et al., 1995; Okada et al., 2000*). Initially, vertical oscillations of the laser beam were achieved through electromechanical or pneumatic devices, which had strict constraints regarding the positioning range and oscillation frequency (*He et al., 2013; Morimoto et al., 2015*).

Recently, alternative solution that enable oscillations of the laser focal plane along the beam propagation direction were developed based on novel fast focusing mirrors (FFMs). These are optical mirrors that can rapidly adjust their surface shape

to change the focal length and focus position of an incident light beam. Oscillations frequencies up to 3 kHz, for several mm oscillation amplitudes, have been obtained with FFMs, significantly higher than previous solutions.

A detailed analysis of the working principle of a FFM was first presented by *Bottner et al.* (*Bottner et al., 2019*), while the integration of such solution into a commercial processing head for cutting and welding application was demonstrated by *Jahn et al.* (*Jahn et al., 2019*). In their study, a 3 kW fiber laser source was employed to process 10 mm thick stainless steel, resulting in a 60% increase in cutting speed through the application of sinusoidal axial oscillations.

A further study by *Herwig et al.* addressed the impact of harmonic axial oscillations on the productivity of fusion cutting process across a variety of materials and thicknesses (*Herwig et al., 2021*). Their findings revealed increases in processing speed for stainless steel, mild steel and aluminum alloy materials of various thicknesses, utilizing a 3 kW laser power.

In this context, the scope of the present work is to explore the effect of dynamic axial oscillations on laser fusion cutting process through both analytical modelling and experimental investigations. While existing literature has primarily focused on dynamic beam shaping employing harmonic oscillations, this study explores the impact of various oscillation waveform patterns on process performance, focusing on their effect on productivity and part quality.

Beyond the conventional sinusoidal oscillations, the waveforms analyzed in this study included triangular, square, ramp-up, and ramp-down patterns.

An analytical model was initially developed to evaluate the laser intensity distribution within the process zone under both static and dynamic conditions. Furthermore, the effect of axial oscillations, superimposed to the cutting direction, was experimentally investigated.

2. Modelling

An analytical model was developed to evaluate the laser intensity distribution within the process zone under both static and dynamic conditions. This model describes the spatial and temporal motion of the laser beam as a function of oscillation patterns, amplitude and frequency.

The spatial intensity distribution under dynamic beam shaping conditions strictly depends on the laser beam motion as well as the intensity distribution of the incident beam. For a conventional laser beam operating in static conditions, its intensity distribution can be well-approximated by a Gaussian function.

Considering an overall power P, Rayleigh length z_R, beam waist radius w_0 in axial position z_0, and centered in (x_0, y_0) coordinates, the analytic expression of its intensity distribution in 3D space could be defined by the well-known formula (*Girerd et al., 2022*):

$$I(x,y,z) = I_{pk} \cdot \exp\left[-2 \cdot \frac{(x-\mathrm{x_0})^2+(y-\mathrm{y_0})^2}{w(z)^2}\right] \quad (1)$$

where the laser peak intensity I_{pk} and beam radius $w(z)$ at position z can be computed as:

$$I_{pk} = \frac{2 \cdot P}{\pi \cdot w(z)^2} \quad (2)$$

$$w(z) = w_0 \cdot \sqrt{1 + \frac{(z-z'(t))^2}{z_R^2}} \quad (3)$$

However, to account for the dynamic motion of the laser beam along its propagation direction (Z-axis), the time-dependent position coordinate $z'(t)$ may be expressed as follows:

$$z'(t) = z_0 + S_z(t) \quad (4)$$

where z_0 denote the initial position coordinate, and $S_z(t)$ represent the oscillation component that account for the axial moving trajectory of the beam focus.

The explicit expression of the time dependent oscillation terms varies according to the selected motion function. For harmonic oscillations this may be simply described by a sinusoidal term:

$$S_z(t) = A \cdot \sin(\omega \cdot t + \phi) \quad (5)$$

The parameter A denote the oscillation amplitude, while the angular frequency is indicated with ω and the phase shift contributions is ϕ.

Although existing literature has primarily focused on dynamic beam shaping employing harmonic oscillations, alternative waveforms such as triangular (TNW), square (SQW), ramp-up (RUW), and ramp-down (RDW) can also be utilized.

The waveforms analytical expressions are here provided:

$$TNW(t) = \frac{8 \cdot A}{\pi^2} \cdot \sum_{n=1}^{n=N} \left\{ \frac{(-1)^n}{(2n \pm 1)^2} \cdot \sin[\omega \cdot (2n-1) \cdot t] \right\} \quad (6)$$

$$SQW(t) = \frac{4 \cdot A}{\pi} \cdot \sum_{n=1}^{n=N} \left\{ \frac{1}{2n-1} \cdot \sin[\omega \cdot (2n-1) \cdot t] \right\} \quad (7)$$

$$RUW(t) = \frac{A}{2} + \frac{2 \cdot A}{\pi} \cdot \sum_{n=1}^{n=N} \left\{ \frac{(-1)^{n+1}}{n} \cdot \sin[\omega \cdot n \cdot t] \right\} \quad (8)$$

$$RDW(t) = \frac{A}{2} - \frac{2 \cdot A}{\pi} \cdot \sum_{n=1}^{n=N} \left\{ \frac{1}{n} \cdot sin[\omega \cdot n \cdot t] \right\} \quad (9)$$

The time-averaged spatial intensity distribution under varying operating conditions can be calculated as the mean value of the previous expression over a single oscillation period T, as:

$$\overline{I(x,y,z)} = \frac{1}{T} \cdot \int_0^T I(x,y,z,t) \cdot dt \quad (10)$$

3. Material and Methods

3.1. Material

This study investigates the fusion cutting of 20 mm thick stainless steel AISI304 material. This was selected due to its industrial relevance in the metal-working industry.

The nominal composition is reported in Table 1.

Table 1: Nominal chemical composition of AISI304 stainless steel (wt%).

Element	C	Si	Mn	P	S	Cr	Ni	Mo	Fe
wt [%]	0.02	0.52	1.50	0.01	0.01	17.30	11.40	2.46	Bal.

3.2. Laser system

The experiments were performed on a customized version of the Fraunhofer IWS laser cutting machine (*Fraunhofer IWS institute, Dresden, Germany*).

An industrial high-power multi-mode fiber laser source that can deliver up to 12 kW of power at a central emission wavelength λ = 1080 µm (*MFMC12000M, Maxphotonics Co., Ltd, Shenzhen, Guangdong, China*) was employed to cut the materials. The transport fiber has a core diameter of 50 µm and is coupled to a Precitec HPSSL (*Precitec GmbH & Co., Gaggenau, Germany*) cutting head, having a collimation and a focusing lens of 100 and 200 mm focal length respectively.

The specifications of the laser system are reported in Table 2.

Table 2: Laser system specifications.

Parameters	Values
Laser power, P [kW]	12.0
Wavelength, λ [nm]	1080
Beam Parameter Product, BPP [mm mrad]	1.57
Collimation lens, f_{col} [mm]	100
Focal lens, f_{foc} [mm]	200
Feeding fiber core diameter, d_{core} [µm]	50
Beam waist diameter, d_{waist} [µm]	100

Dynamic beam shaping functionality was achieved by integrating a single fast focusing mirror (*FFM, Zwobble scanner, ROBUST AO GmbH, Jena, Germany*) into the conventional Precitec HPSSL cutting head, as represented in Figure 1.

The scanning system consisted of a single mirror that can rapidly adjust its surface shape to change the focal length and focus position of an incident laser beam.

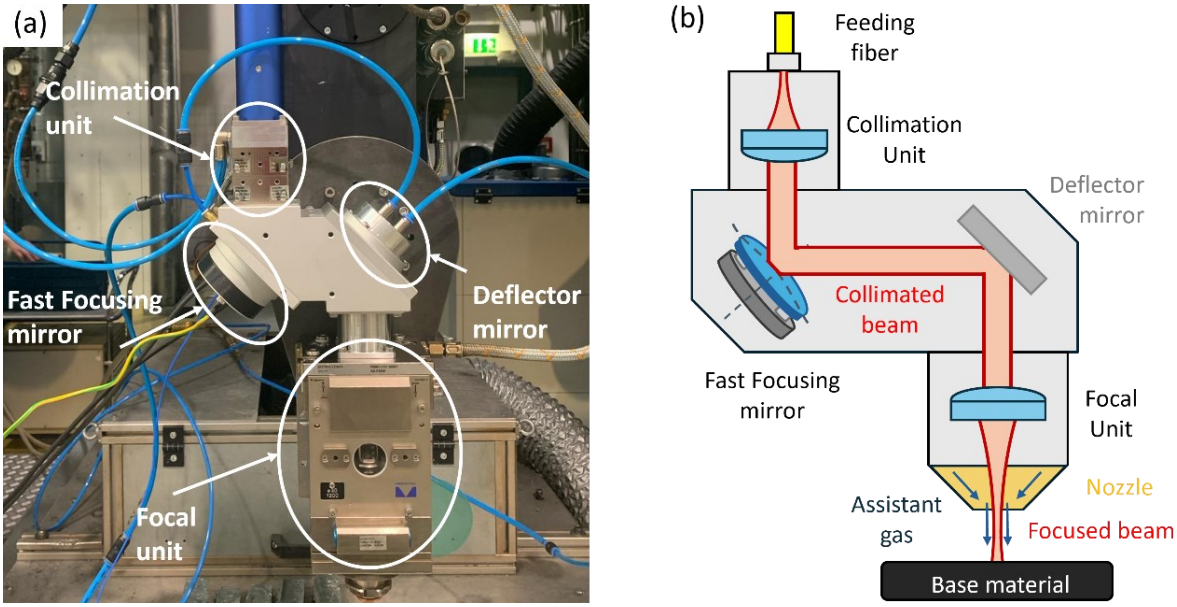

Figure 1: Precitec HPSSL cutting head equipped with a ROBUST AO Zwobble mirror: (a) photo; (b) schematic representation.

3.3. Experimental plan

The present study investigates the effect of laser beam axial oscillations on processing speed and part quality for 20 mm thick stainless steel AISI304.

An overview of the process parameters applied for cutting this material in static conditions is provided in Table 3. These parameters are obtained from preliminary experimental investigations. The nominal speed corresponds to the maximum cutting rate that can be achieved while still maintaining an acceptable level of part quality.

Table 3: Experimental design for 20 mm thick AISI304 laser fusion cutting process under static and dynamic axial oscillations.

Process parameters	**Values**	
Assistant gas	N2	
Gas pressure, pr [bar]	17	
Stand-off distance, $d_{stand\text{-}off}$ [mm]	0.7	
Nozzle diameter, d_{nozzle} [mm]	3.0	
Laser power, P [kW]	6.0	
	Reference	**Variable factors**
Oscillation patterns	Static	Sinusoidal, Triangular, Square, Ramp-up, Ramp-down
Focal position, FP [mm]	-12.0	-4.0; -6.0; -8.0; -10.0
Oscillation amplitude, A [mm]	n.a.	1.0; 3.0; 5.0; 7.0
Oscillation frequency, f [kHz]	n.a.	0.1; 0.5; 1.0
Cutting speed, v [m/min]	0.70	0.60; 0.65; 0.70; 0.75; 0.80; 0.85; 0.90; 0.95; 1.0

The experimental plan was designed to assess the influence of various laser oscillation waveform patterns on the productivity and part quality of 20 mm thick stainless steel AISI304. The waveforms studied included sinusoidal, triangular, square, ramp-up, and ramp-down patterns. Cutting experiments were conducted with varying combinations of oscillation amplitudes and frequencies. However, it is worth noticing that these were constrained by the mirror dynamics.

Specifically, a maximum oscillation frequency of 1.5 kHz could be achieved for sinusoidal and triangular waveforms. In contrast, ramp-up and ramp-down waveforms were limited to a frequency of 0.5 kHz, whereas the square waveform could only achieve a frequency of 0.1 kHz. Five levels of oscillation amplitudes were tested, ranging from 1 to 7 mm.

To investigate the productivity of the process under dynamic beam shaping conditions, cutting speeds were incrementally increased from the nominal value obtained under static reference conditions. Speed increments of 0.05 m/min were applied,

for a total of 9 speed levels. A stand-off distance of 0.7 mm and a gas pressure of 17 bar were maintained consistently across all experiments. A nozzle with a diameter of 3.0 mm was used. The laser power was kept fixed at 6.0 kW, while the focal position was adjusted between 4.0 mm and 10.0 mm below the material surface.

The fixed and variable process parameters are outlined in Table 3.

3.4. Characterization and measurement

The samples were visually inspected and grouped under the following three categorical conditions:

- Successful cut: the molten material is ejected, leading to complete material separation.
- Plasma cut: unstable laser cutting process conditions may induce plasma formation, resulting in complete material separation but with low cut-edge quality.
- Loss of cut: the molten material is not ejected from the kerf but resolidified, preventing separation.

Representative optical microscope images of these conditions are reported in Figure 2 (loss of cut shown in a top view, while plasma and successful cut showing the kerf surface).

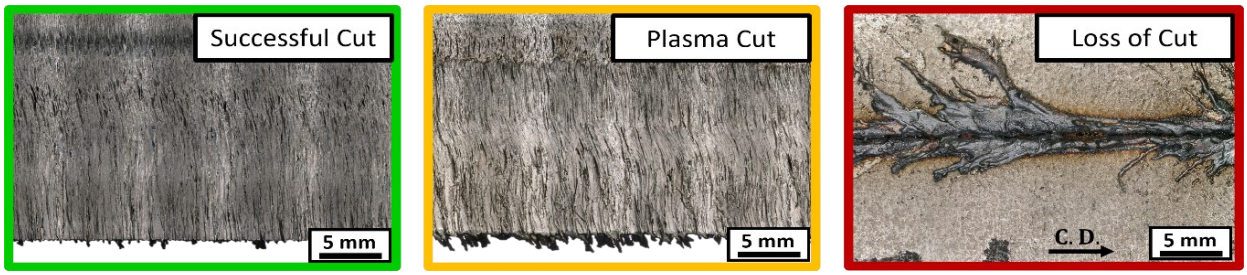

Figure 2: Qualitative cutting results for 20 mm thick AISI304: Successful Cut (in green); Plasma Cut (in yellow) and Loss of Cut (in red).

For successful conditions, process productivity was evaluated considering the highest cutting rate achievable while still maintaining acceptable cut quality. Moreover, the part quality was assessed by extracting the burr height (h) and cut-edge roughness (Rz) defects.

The surface roughness was measured with a Jenoptik Waveline W20 profilometer (*Jenoptik AG, Jena, Thüringen, Germany*) equipped with an TKU-300 feeler and a 5 µm radius tip. In accordance with the UNI EN ISO standards for profile measurements, the acquired sample primary profile is filtered with a 2.5 mm cut-off wavelength. The resulting mean peak-to-valley height roughness profile, Rz, was extracted. The roughness profile was measured at three different positions along the cut-edge surface (see Figure 3a): at the center of the material and 1 mm above and below the top and bottom surface respectively. Three measurements were taken at each position, and the mean and standard deviation values were computed.

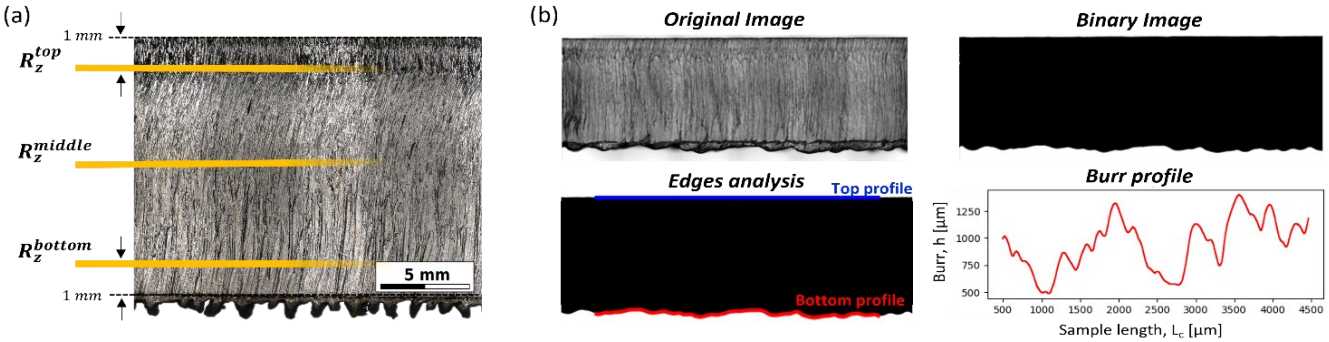

Figure 3: (a) Surface roughness. Three different positions along the cut-edge surface: the center of the material and 1 mm above and below the top and bottom surface respectively. (b) Burr estimation procedure: Original microscope image; Binary image; Detection of the top and bottom cut-edge profiles and rotation for misalignment compensation; Extraction of the burr profile along the sample length.

The Keyence VHX digital microscope (*Keyence corporation, Osaka, Japan*) was employed for high-resolution imaging of the samples, while the burr defect was extracted through a Python image processing algorithm (see Figure 3b). The colored microscope image of the cut-edge profile was first converted into a grayscale image and then to a binary matrix by applying a thresholding operation based on pixel intensity. The top and bottom sample edges were identified, and the matrix image

was rotated to compensate for misalignment. Subsequently, the difference between the two profile edges was computed and by subtracting the material thickness, a reliable estimation of the burr defect h along the entire sample profile was identified.

4. Results

4.1. Laser intensity distribution

Based on the analytical model presented in section 2, the laser intensity distributions for static conditions ($\mathrm{A} = 0$ mm) and the time-averaged intensity distribution under various axial oscillation waveforms (SNW, TNW, SQW and RUW) with fixed amplitudes of $\mathrm{A} = 7$ mm and frequency $f = 1.0$ kHz are shown in Figure 4.

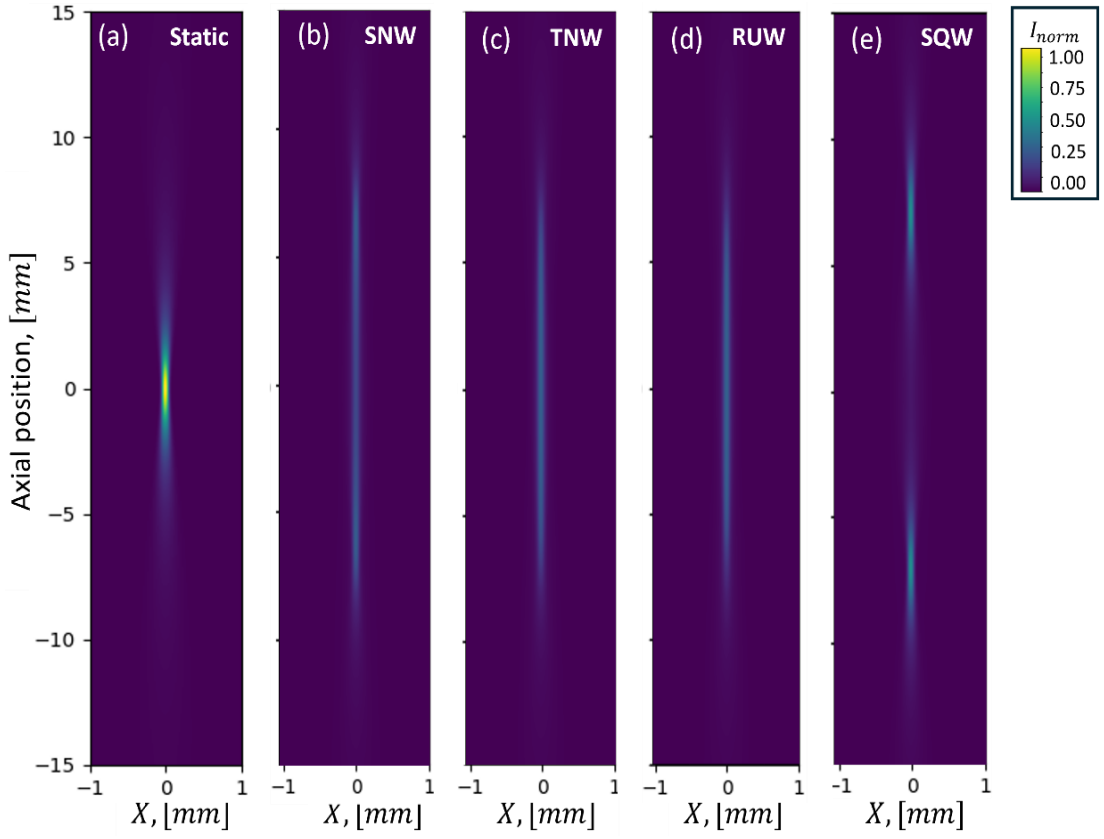

Figure 4: Normalized time-averaged laser intensity distribution for: (a) static gaussian beam, (b) sinusoidal SNW, (c) triangular TNW, (d) ramp-up RUW and square SQW waveforms with 7.0 mm oscillation amplitudes and 1.0 kHz frequency.

For better comparison, the intensity distributions associated with the different oscillation patterns are normalized with respect to the peak intensity of the static condition, according to the following expression:

$$I_{norm} = \frac{\overline{I(x,y,z)}}{I_{pk}^{static}} \tag{11}$$

Additionally, the beam spot size and peak intensities along the axial direction are displayed in Figure 5. While triangular and ramp-up oscillation patterns yield beam radius and peak intensity distributions similar to those of sinusoidal oscillation, the square waveform produces a distinct profile.

Specifically, it results in a beam radius and peak intensity distribution along the axial propagation direction that closely resembles the effect of diffractive optical elements designed to generate a double focal point. In this case, the highest peak intensity occurs at the inversion point positions.

It is evident that axial oscillations significantly influence both laser intensity distribution and beam dimensions. Specifically, they result in a more homogeneous intensity distribution along the beam propagation direction and an increased

Rayleigh length. This effect is expected to enhance process efficiency and increase processing speed, as discussed by *Mahrle and Beyer* (*Mahrle and Beyer, 2007*).

Moreover, the increased average beam diameter leads to a wider kerf, which facilitates the coupling of the assist gas to the kerf. This improved gas flow may enhance the removal of molten material and, as a result, positively impact the quality of the cut samples (*Borkmann et al., 2021)*.

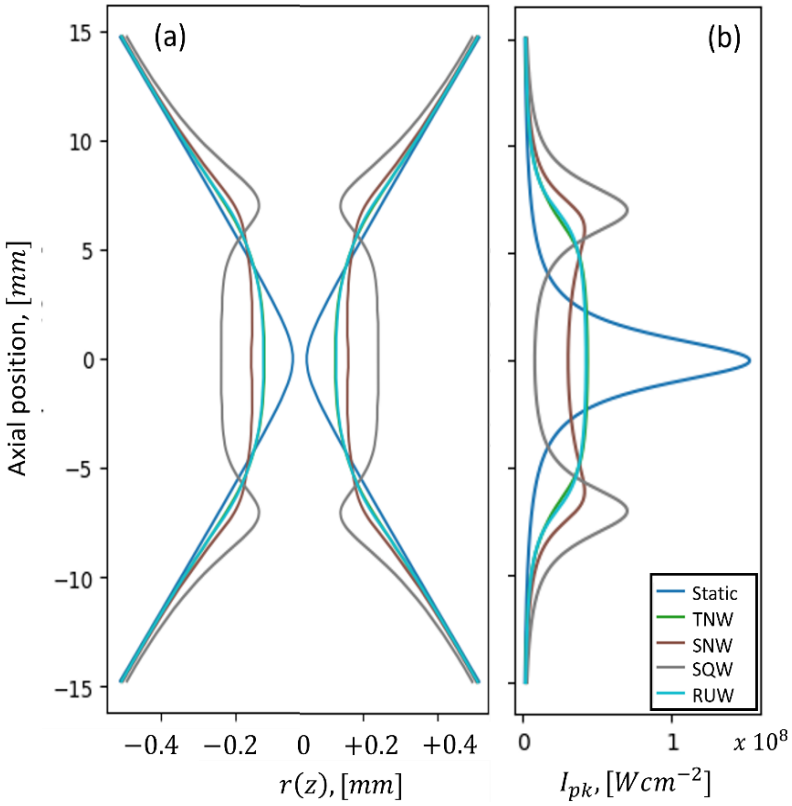

Figure 5: (a) Beam radius and (b) peak intensity along laser propagation direction for different waveforms ($A = 7\ mm$, $f = 1.0\ kHz$).

4.2. Experimental results

The samples resulting from the experimental plan described in section 3.3 were visually inspected and classified into three categories: Successful cut, Plasma cut and Loss of cut. Moreover, for each waveform pattern, the samples achieving the highest cutting rate while maintaining acceptable part quality were identified.

Optical microscope images of the cut-edges under these selected process conditions are shown in Figure 6a, the corresponding cutting rates are represented in Figure 6b, and the relevant process parameters are summarized in Table 4.

Table 4: Laser fusion cutting process parameters for 20 mm thick AISI304 stainless steel.

Oscillation patterns	**Static**	**Sinusoidal**	**Triangular**	**Square**	**Ramp-Up**	**Ramp-Down**
Focal position, FP [mm]	-12.0	-6.0	-6.0	-10.0	-6.0	-6.0
Oscillation amplitude, A [mm]	n.a.	7.0	7.0	5.0	7.0	7.0
Oscillation frequency, f [kHz]	n.a.	0.1	0.5	0.1	0.1	0.5
Cutting speed, v [m/min]	0.70	0.80	0.85	0.70	0.80	0.85

Under static conditions, a processing speed of 0.70 m/min was achieved with the focal position set 12.0 mm below the material surface. When applying sinusoidal axial oscillation, the speed increased to 0.80 m/min, with the focal position oscillating around 6.0 mm below the upper material surface. The oscillation frequency was 0.1 kHz with an amplitude of 7.0 mm. The same processing speed of 0.80 m/min was obtained using a ramp-up waveform with identical amplitude and frequency.

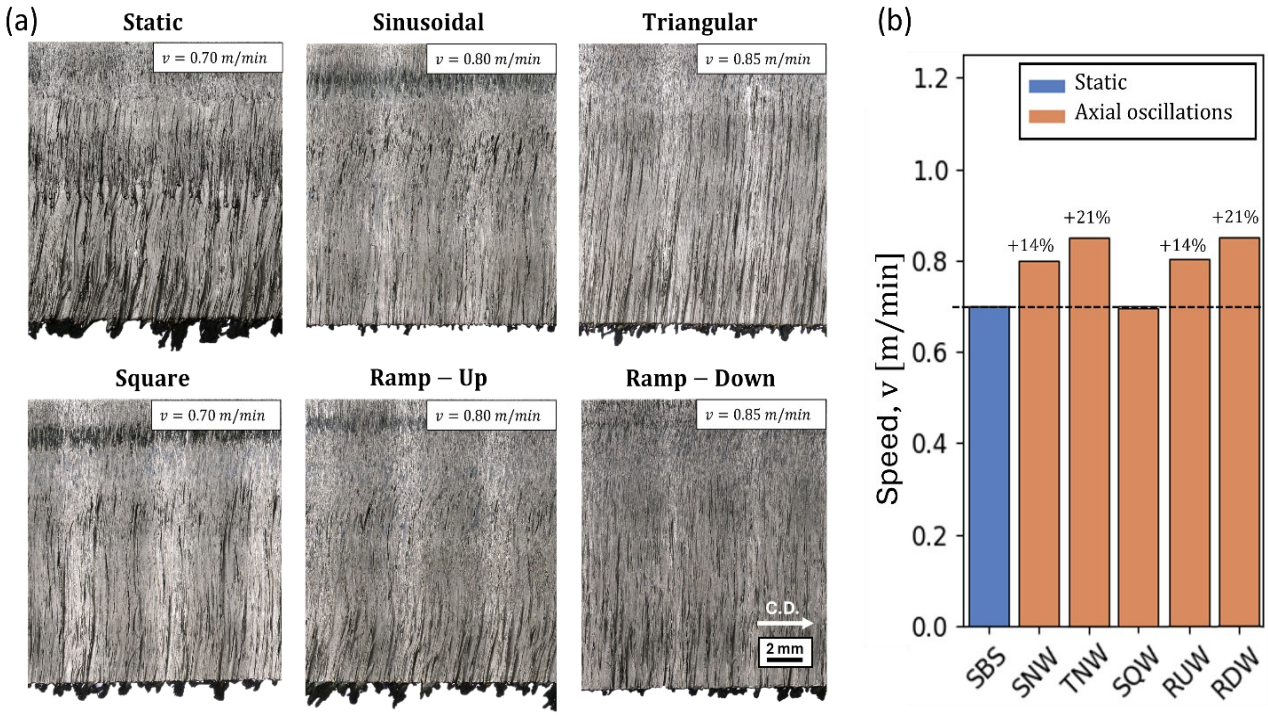

Figure 6: (a) Optical microscope cut-edges images and (b) cutting speeds of selected process conditions under different axial oscillation waveforms: Static (in blue) and Dynamic conditions (in brown). Sinusoidal, Triangular, Square, Ramp-up and Ramp-down.

In contrast, triangular and ramp-down waveforms yielded further improvements, reaching processing speeds of up to 0.85 m/min. These employed an oscillation frequency of 0.5 kHz and an amplitude of 7.0 mm, with the focal position still oscillating around 6.0 mm below the material surface.

For square wave oscillation, a speed of 0.70 m/min was recorded, equivalent to the static condition. In this case, the focal position was centered at 10.0 mm below the surface, with an oscillation frequency of 0.1 kHz and an amplitude of 5.0 mm.

Furthermore, the results related to part quality obtained under static (in blue) and dynamic beam shaping conditions (in brown) are presented in Figure 7. Specifically, Figure 7a shows the burr height, while Figure 7b reports the surface roughness measured at the upper, central and lower regions of the material thickness.

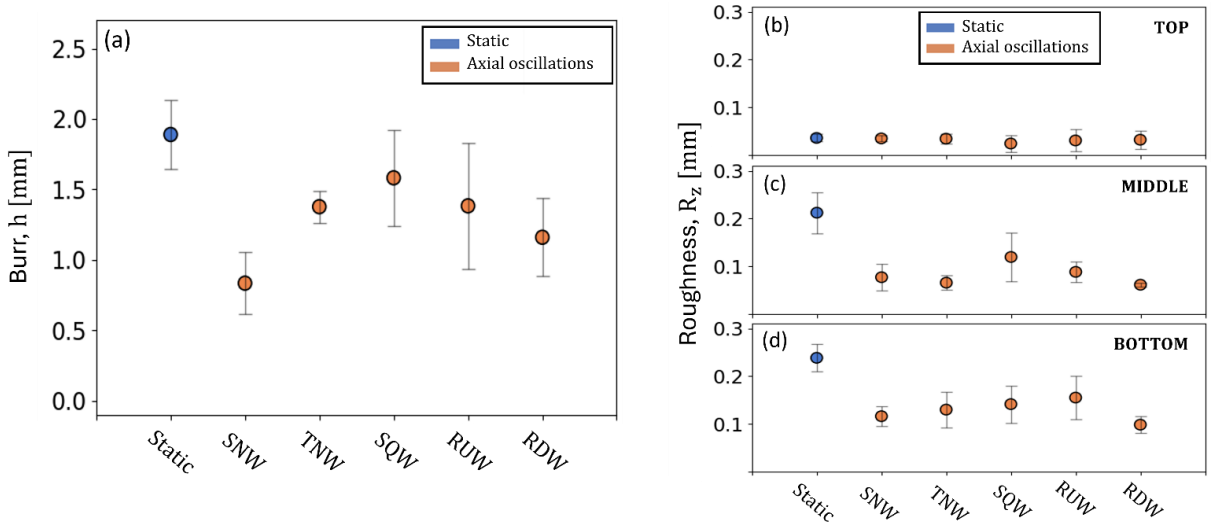

Figure 7: Part quality for the processing of 20 mm thick stainless steel AISI304: (a) burr height; (b) top, (c) middle and (d) bottom roughness profile. The mean values with a three standard deviation error bar are reported.

While the burr height was approximately 1.9 mm under static beam conditions, a reduction was observed across all dynamic beam shaping strategies. Specifically, triangular (TNW), square (SQW), ramp-up (RUW), and ramp-down (RDW) waveforms resulted in burr heights ranging between 1.2 mm and 1.6 mm. The lowest burr height, 0.9 mm, was achieved using sinusoidal oscillations, which enabled a significant reduction in burr formation compared to the static case.

Regarding the roughness profile, no significant difference was observed at the top measurement position between static and dynamic conditions. However, a notable reduction in surface roughness was recorded at the middle and bottom positions for all tested waveforms. This improvement is further supported by the microscope images in Figure 6, which reveal a more uniform cut-edge surface achieved through the application of axial oscillations.

5. Conclusions

The present work explores the impact of various axial oscillation waveforms, namely sinusoidal, triangular, square, ramp-up, and ramp-down patterns, on the laser fusion cutting process through analytical modelling and experimental investigations.

An analytical model was first developed to evaluate the laser power distribution within the process zone for each oscillation pattern. Simulation results indicate that axial oscillations substantially affect both the laser intensity distribution and beam geometry. In particular, the oscillations enable a more homogeneous intensity profile along the beam propagation direction and extend the Rayleigh length, which may lead to more uniform laser power absorption throughout the material thickness.

Furthermore, the effect of axial oscillations superimposed on the cutting direction was experimentally investigated in the processing of 20 mm thick AISI304 stainless steel. The experimental results demonstrate notable improvements in process performance, with axial oscillation enabling increased processing speeds while simultaneously enhancing part quality through reduction in both burr height and surface roughness.

While the square waveform improves part quality at the same processing speed as the reference static condition, all other waveform patterns yield significant improvements in both part quality and processing speed. Specifically, the best process performances were obtained using sinusoidal and ramp-down axial oscillation patterns. Sinusoidal oscillations led to a 14% increase in cutting speed and a 58% reduction in burr height, whereas the ramp-down waveform achieved a 21% increase in speed and a 42% reduction in burr height.

Additionally, both waveforms led to a substantial reduction in surface roughness, with decreases of approximately 65% and 55% in the central and lower regions of the material thickness, respectively.

Acknowledgments

The authors gratefully acknowledge the Italian Ministry for University and Research (MUR) for supporting the research via the National Plan for Recovery and Resilience (PNRR).

References

D'Arcangelo S, Busatto M, Caprio L, Previtali B, Demir AG. Hybrid use of a robotic welding system in remote laser separation of thin-sheet Al casings for the recycling of battery packs. Journal of Laser Applications. 2024.

Fuse K. Beam Shaping for Advanced Laser Materials Processing: Generation of shape and intensity profile of laser beam with aspheric and diffractive optics. Laser Technik Journal. 2015.

Müller A, Goecke SF, Sievi P, Albert F, Rethmeier M. Laser Beam Oscillation Strategies for Fillet Welds in Lap Joints. Physics Procedia. 2014.

Huang J, Qin Q, Wang J, Fang H. Two Dimensional Laser Galvanometer Scanning Technology for Additive Manufacturing. IJMMM. 2018.

Goppold C, Herwig P, Stoffel D, Bach M. Tip-tilt piezo platform scanner qualifies dynamic beam shaping for high laser power in cutting applications. 2019;

Kardan M, Levichev N, Castagne S, Duflou JR. Cutting thick aluminum plates using laser fusion cutting enhanced by dynamic beam shaping. Journal of Laser Applications. 2023.

Gropp A, Hutfless J, Schuberth S, Geiger M. Laser beam cutting. Opt Quant Electron. 1995.

Okada T, Ebata K, Shiozaki M, Kyotani T, Tsuboi A, Sawada M, et al. Development of adaptive mirror for CO2 laser. Proceedings of SPIE - The International Society for Optical Engineering. 2000.

He D, Shinshi T, Nakai T. Development of a maglev lens driving actuator for off-axis control and adjustment of the focal point in laser beam machining. Precision Engineering. 2013.

Morimoto Y, He D, Hijikata W, Shinshi T, Nakai T, Nakamura N. Effect of high-frequency orbital and vertical oscillations of the laser focus position on the quality of the cut surface in a thick plate by laser beam machining. Precision Engineering. 2015.

Böttner P, Reinlein C, Jahn A, Herwig P, Goppold C, Stoffel D, et al. Design, manufacturing and test of a highly dynamic piezo- driven metal mirror for laser material processing. 2019.

Jahn A, Goppold C, Herwig P, Reinlein C, Boettner P, Stoffel D, et al. High dynamic beam shaping by piezo driven modules for efficient and high quality laser beam cutting and welding. 2019.

Herwig P. Laser Sawing with piezo-driven adaptive mirror. 2021.

Girerd T, Madrigal AG, Clare A, Norton A. Lissajous curve oscillations in laser welding. Procedia CIRP. 2022.